PREPARED FOR THE U.S. DEPARTMENT OF ENERGY,
UNDER CONTRACT DE-AC02-76CH03073

PPPL-3765
UC-70

PPPL-3765

Hall MHD Modeling of Two-dimensional Reconnection: Application to MRX Experiment

by

V.S. Lukin and S.C. Jardin

January 2003

PPPL
PRINCETON PLASMA
PHYSICS LABORATORY

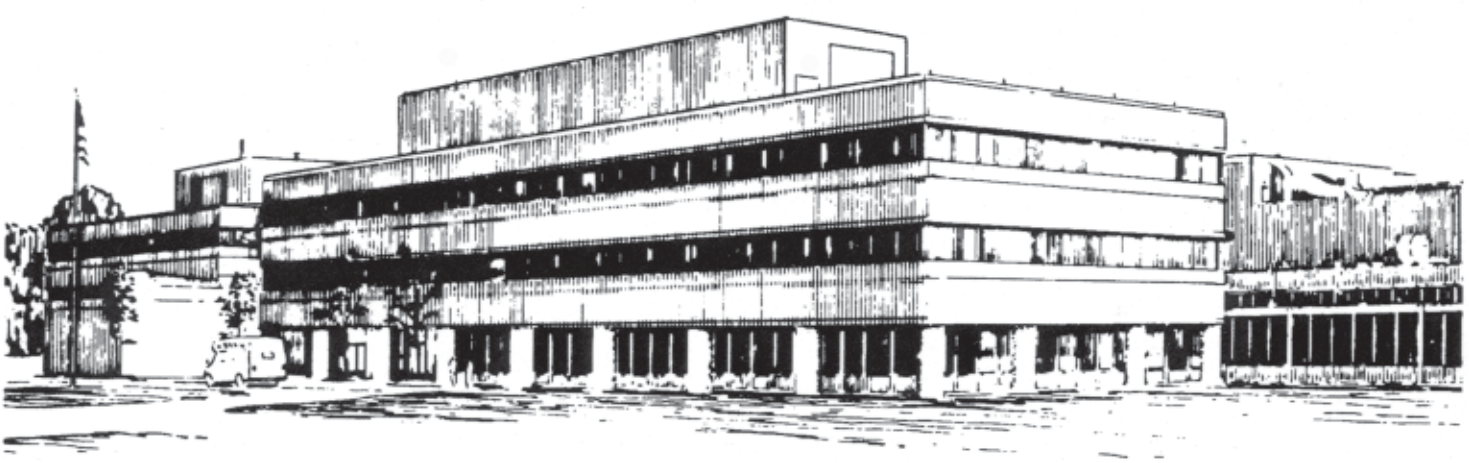

PRINCETON PLASMA PHYSICS LABORATORY
PRINCETON UNIVERSITY, PRINCETON, NEW JERSEY

PPPL Reports Disclaimer

Availability

This report is posted on the U.S. Department of Energy's Princeton Plasma Physics Laboratory Publications and Reports web site in Fiscal Year 2003. The home page for PPPL Reports and Publications is: http://www.pppl.gov/pub_report/

DOE and DOE Contractors can obtain copies of this report from:

U.S. Department of Energy
Office of Scientific and Technical Information
DOE Technical Information Services (DTIS)
P.O. Box 62
Oak Ridge, TN 37831

Telephone: (865) 576-8401

Fax: (865) 576-5728

Email: reports@adonis.osti.gov

This report is available to the general public from:

National Technical Information Service
U.S. Department of Commerce
5285 Port Royal Road
Springfield, VA 22161

Telephone: 1-800-553-6847 or
(703) 605-6000

Fax: (703) 321-8547

Internet: http://www.ntis.gov/ordering.htm

Hall MHD modeling of two-dimensional reconnection: application to MRX experiment.

V. S. Lukin and S. C. Jardin
Princeton Plasma Physics Laboratory
Princeton University
Princeton, NJ 08543

December 22, 2002

Abstract

A two-dimensional resistive Hall magneto-hydrodynamics (MHD) code is used to investigate the dynamical evolution of driven reconnection in the Magnetic Reconnection Experiment (MRX). The initial conditions and dimensionless parameters of the simulation are set to be similar to the experimental values. We successfully reproduce many features of the time-evolution of magnetic configurations for both co- and counter-helicity reconnection in MRX. The Hall effect is shown to be important during the early dynamic X-phase of MRX reconnection, while effectively negligible during the late "steady-state" Y-phase, when plasma heating takes place. Based on simple symmetry considerations, an experiment to directly measure the Hall effect in MRX configuration is proposed and numerical evidence for the expected outcome is given.

1 INTRODUCTION

A large number of numerical studies have been undertaken in recent years in order to better our understanding of the reconnection process and the detailed structure of reconnection sites (see, for example [1, 2, 3, 4, 5, 6, 7]). Both 3D and 2D geometries with various imposed symmetries have been investigated. And while fully three dimensional reconnection remains poorly defined, there is now general agreement on what the basic structure of two dimensional reconnection should be [5, 6, 7, 8, 9, 10]. Localization of the reconnection region [10], achieved in magneto-hydrodynamics (MHD) by including collisionless effects in the Ohm's law, seems to be responsible for the observed fast reconnection rates in the collisionless regime [5, 6, 7, 9].

In particular, inclusion of the Hall term in the generalized Ohm's law has been shown to result in collapse of Y-shaped reconnection layer [11] to an X-point structure with characteristic quadrupolar out-of-plain magnetic field (Hall magnetic field) arising around the reconnection site [5, 7]. Most recently, this theoretical prediction was confirmed by *in situ* measurements of Hall magnetic fields at reconnection sites in the Earth's magnetotail [12] and subsolar magnetopause [13].

However, there is still a large gap in our understanding of even 2D magnetic reconnection, as most of the numerical studies [1, 2, 3, 4, 6, 7, 8, 9] remain unrelated to the experimental effort dedicated to reproducing and describing reconnection in the laboratory setting [14, 15, 16, 17, 18, 19, 20, 21, 22]. It is easily observed by comparing the results of numerical studies cited above, that initial and boundary conditions applied to the problem greatly influence the time-evolution of the structure of the reconnection region. Though such a conclusion cannot be surprising, it necessitates application of computational codes to specific experiments, to both improve our ability to interpret and compare theoretical predictions against experimental data. In one such effort, an earlier version of the same code as used in the present study, was successfully adapted to the geometry of the Swarthmore Spheromak Experiment [23, 24].

In this paper, we use Hall MHD to model both global and local reconnection dynamics observed in the Magnetic Reconnection Experiment (MRX) [21]. In Section 2, we describe the basic structure of the code, the initial conditions and the time-evolution of the boundary conditions applied to the simulation domain. In Section 3, resistive MHD simulation results are compared to experimental data. In Section 4, symmetry properties of Hall MHD and its relevance to the MRX experiment are discussed. In Section 5, results of the Hall MHD model are presented

and a comparison of co- and counter- helicity reconnection configurations [21] are made. Finally, based on the presented evidence, in Section 6 we propose a qualitative description of Hall mediated dynamics of reconnection in MRX and propose an experiment to directly observe the Hall effect in MRX.

2 Hall MHD model and MRX

We employ a two-dimensional axisymmetric resistive compressible Hall MHD code – modified TRIangular Magneto-hydrodynamics (TRIM)[25], to simulate the time-evolution of electro-magnetic fields, momentum density and plasma density in MRX. In doing so, we solve the following set of resistive Hall MHD equations in cylindrical geometry with no-slip perfectly conducting boundaries:

$$\frac{\partial \rho}{\partial t} + \nabla \cdot (\rho \mathbf{v}) = 0, \tag{1}$$

$$\frac{\partial \mathbf{A}}{\partial t} = -\mathbf{E}, \tag{2}$$

$$\mathbf{E} = -(\mathbf{v} - \lambda \mathbf{J}) \times \mathbf{B} + \eta \mathbf{J}, \tag{3}$$

$$\frac{\partial (\rho \mathbf{v})}{\partial t} + \nabla \cdot (\rho \mathbf{v}\mathbf{v}) = \mathbf{J} \times \mathbf{B} - \nabla p + \rho \nu \nabla^2 \mathbf{v}, \tag{4}$$

$$\frac{\partial U}{\partial t} = -\nabla \cdot \left[\left(\frac{\rho v^2}{2} + \frac{\gamma}{\gamma - 1} p \right) \mathbf{v} + \frac{\mathbf{E} \times \mathbf{B}}{\mu_0} \right] - R_{loss}. \tag{5}$$

In the TRIM implementation, the three components of the vector potential $\mathbf{A}$, the three components of the momentum density $\rho \mathbf{v}$, the density ρ and total energy $U = \rho v^2/2 + B^2/2\mu_0 + p/(\gamma - 1)$, are propagated in time on an unstructured grid of triangles in the $\hat{r} \times \hat{z}$ plane. The magnetic field $\mathbf{B}$ and current density $\mathbf{J}$ are calculated from the vector potential using $\mathbf{B} = \nabla \times \mathbf{A}$ and $\mathbf{J} = (\nabla \times \mathbf{B})/\mu_0$. Cylindrically symmetric boundary conditions and initial configuration of electromagnetic fields, plasma density, plasma pressure and momentum density, together with several constant parameters, such as the Lundquist number $S = L_A^2 \mu_0 / \eta \tau_A$, the Hall coefficient $\lambda = 1/e\bar{n}$ and viscosity $\nu = 10^{-3}$ determine the time evolution of the calculated parameters [25].

In the present studies, we found it important to adjust the simple adiabatic equation of state ($\gamma = 5/3$) by including the impurity radiation. In doing so,

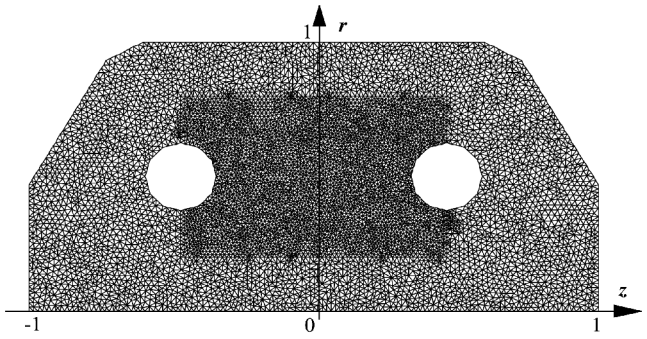

Figure 1: The computational mesh used by TRIM to model MRX.

we used polynomial fits [26] to calculate the local rate of energy loss R_{loss} as a function of local temperature and plasma density. We assumed carbon to be the dominant impurity at about 10% of plasma density.

To estimate the desired value of λ, we use the average electron density in the MRX reconnection layer of $\bar{n} = 6 \times 10^{19} m^{-3}$, which corresponds to a normalized value of $\lambda' = 2.4 \times 10^{-2}$. However, since in the modified TRIM code the Hall effect is implemented explicitly, there is a severe restriction on the maximum stable time-step for a given spatial resolution, as a function of the λ' parameter. As a result, for practical considerations, we limit λ' to no more than about 4×10^{-3}. Note that although the electron pressure term ∇p_e normally present in the Ohm's law (Eq.3) and generally considered to be of the same order as the Hall term, is neglected in the present study in the low β_e limit [5].

Figure 1 shows the geometry of the computational domain. The triangle mesh density is on the order of 10^4 per L_0^2, where $L_0 = 0.75m$ is the major radius of the device and the unit length in the simulation. About 2.5 times higher mesh density is used in the region between the flux-cores, where reconnection itself takes place and where most of the available experimental data in MRX comes from. The boundary conditions implemented at the flux-cores allow for imposed tangential electric field both in the toroidal $\hat{\phi}$ direction and in the poloidal $\hat{r} \times \hat{z}$ plane.

We initialize the simulation with constant and uniform plasma density and pressure. The only initial magnetic field is a uniformly imposed B_z, provided in the experiment by outside equilibrium field coils. As in the experiment, the time-evolution of the simulation can be separated into three stages. (See Fig. 6 in [21]. Note that $t = 0$ time in the simulation, in the experiment corresponds to $t = 120\mu s$ in ref.[20, 21], and to $t = 100\mu s$ in ref.[17, 18, 19].)

(1) Quadrupolar poloidal magnetic field is injected into the flux-conserver by

setting $E_\phi = -80.5V/m$ at the flux-core boundaries from $t = 0$ to $t = 103\mu s$. Artificially high resistivity is used to model the pre-ionized gas in MRX.

(2) Co-/counter- directed toroidal magnetic field is injected at the two flux-cores by imposing same/opposite directed poloidal tangential E-field ($E_{tan} = +/-82.8V/m$) at $t = 90.5\mu s$. (In the experiment, this process is also responsible for creating the plasma [21].)

(3) Reconnection is induced by pulling the poloidal magnetic flux back onto the flux-cores. To do so, we set $E_\phi = 80.5V/m$ at the flux-core boundaries from $t = 120\mu s$ to $t = 256\mu s$. We also maintain a poloidal tangential E-field ($E_{tan} = +/-82.8V/m$) until $t = 174.6\mu s$. At $t = 120\mu s$, we also reset the plasma pressure and density to be uniform with $n_0 = 2.25 \times 10^{19} m^{-3}$ and $p = 7J/m^3$.

The first two stages are only included to set up the initial conditions for the third phase of the simulation, when the reconnection processes of interest take place and when all the comparisons with experimental data can be made.

Following Watanabe *et.al.* [27], the resistivity just around the flux-cores is enhanced during the pull-reconnection phase to prevent the development of unphysically-large induction currents in those regions:

$$\eta = \eta' + \frac{1}{2}\eta' C_\eta [e^{-\frac{(r_1 - r_c)^2}{(2r_c)^2}} + e^{-\frac{(r_2 - r_c)^2}{(2r_c)^2}}], \tag{6}$$

where r_1 and r_2 are the distances to the centers of the two flux-cores, r_c is the minor radius of a flux-core, and C_η is the enhancement coefficient, taken to be $C_\eta = 20$. Otherwise uniform resistivity is used with $\eta' = 1/S' = 1/1000$. (We take the Alfvén length scale to be the approximate length of the MRX current layer $L_A = 15cm$ and the Alfvén time to be $\tau_A = 1.33\mu s$ so that the physically meaningful value of the Lundquist number is $S = 325$.) It should be noted that unlike Watanabe *et. al.*, we restrict the region of enhanced resistivity to a very limited area right outside of the flux-cores, which allows for much more realistic modeling of the MRX experiment.

3 Resistive MHD vs. MRX

One of the aims of the simulation work described in this paper is to reproduce and understand the results of the experimental measurements conducted in MRX in its present setup. For the initial studies, we have chosen to eliminate the Hall term from the evolution equations (i.e. set $\lambda = 0$ in Eq.3), in order provide a baseline for the subsequent studies. The effect of keeping this term is discussed

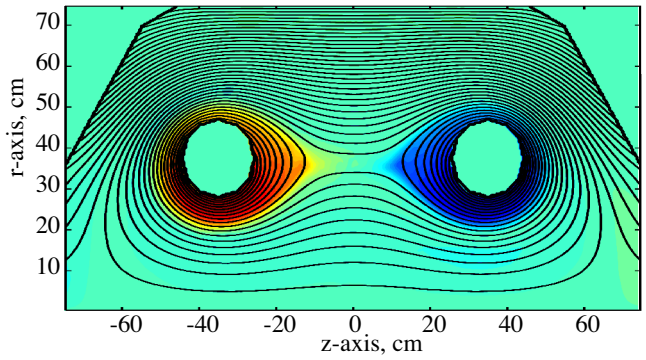

Figure 2: Contours of poloidal magnetic flux overlaid on the color-map of toroidal B-field at $t = 228.9\mu s$ during counter-helicity reconnection.

in the next section. In this section, we also limit ourselves to presenting only counter-helicity reconnection results, as most of the MRX data is taken in that configuration. (We regard the experimental results referred to as "null-helicity" because of apparent lack of the toroidal B-field during the late phase of MRX reconnection (see ref.[17, 18, 19, 20, 21]), as counter-helicity, based on the initial presence of opposing B_ϕ fields necessary to create the plasma.)

In Figure 2, we show contours of poloidal flux Ψ overlaid on the color-map of toroidal magnetic field B_ϕ over the whole computational domain during the steady-state phase of reconnection at $t = 228.9\mu s$. It is observed, that during this phase the reconnection region takes the Y-shape of a long current sheet. The time-evolution of the reconnection region is shown in Figure 3, where four snapshots of the Ψ contours can be compared to the experimental data in Fig.1(c) of Yamada *et. al.*[18]. The time shift of about $35\mu s$ between the MRX experiment and the MHD simulation should be attributed to the slight difference in the implemented time-sequence of the driving flux-core E-fields, which is due to our inability to model plasma break-down.

We further concentrate on the current layer in Figure 4, where radial profiles of toroidal reconnection current J_ϕ and plasma temperature T across the layer at three points in time are shown. These can be compared to Fig.2 of ref.[18] and Fig.3.5 of ref.[19]. Slow radial inward movement of the current layer in the simulation is apparent in Figure 4. This movement is due to the toroidal nature of the device. In the experiment it is controlled by the time varying external equilibrium B_z field. We also include an external uniform B_z field in the simulation, but are unable to vary it in time, which results in the slow radial shift of the current layer.

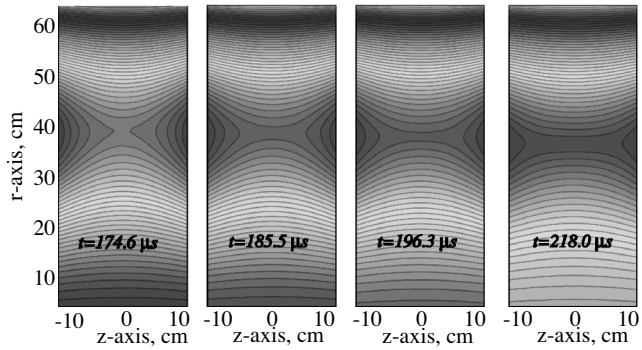

Figure 3: The evolution of poloidal magnetic flux from X-point to Y-shaped reconnection region during counter-helicity reconnection.

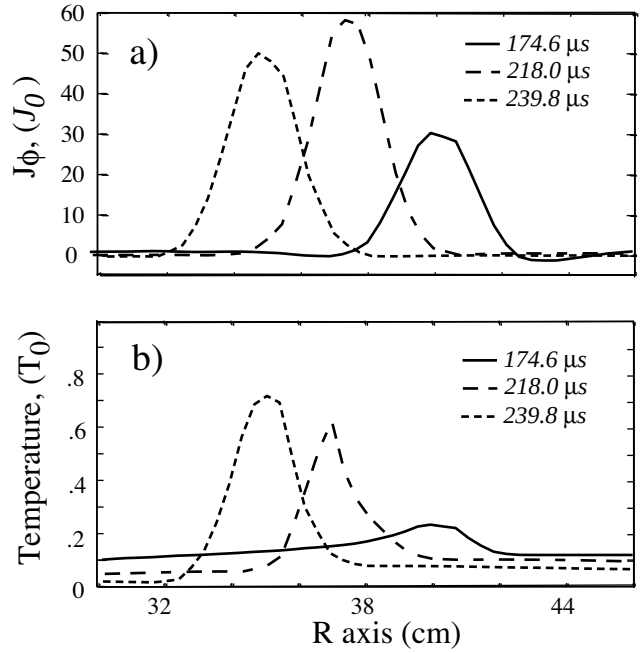

Figure 4: The radial profiles of (a) current density ($J_0 = 16.0kA/m^2$) and (b) plasma temperature ($T_0 = 24.8eV$) through the center of the reconnection layer at three instances during the resistive MHD simulation of counter-helicity reconnection.

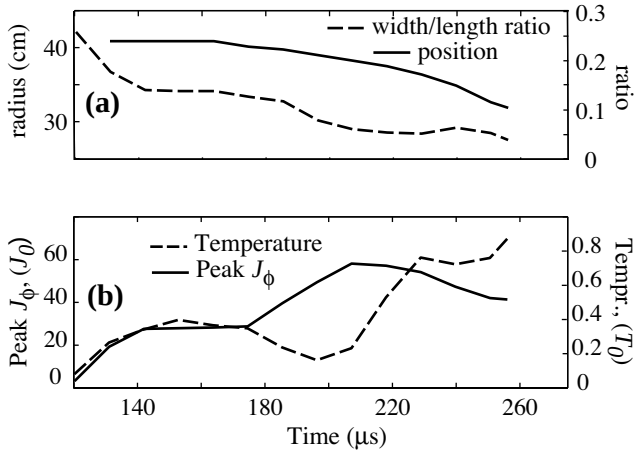

Figure 5: The time history of (a) radial position and width-to-length ratio of the reconnection layer and (b) peak J_ϕ and plasma temperature in the layer during the resistive MHD simulation of counter-helicity reconnection ($J_0 = 16.0kA/m^2$).

The time histories of the exact radial position and a measure of the shape of the reconnection layer are shown in Figure 5(a). We calculate the width-to-length ratio of the reconnection region by measuring the distances it takes poloidal flux Ψ to change by 1% from its X-point value in vertical and horizontal directions. Peak J_ϕ and layer averaged plasma temperature, are shown in Figure 5(b). The two plots in Fig.5(b) can be compared to experimental data in Fig.4 of ref.[20] and Fig.5 of ref.[18]. We observe that in the simulation, as well as in the experiment, the growth of the reconnection J_ϕ and the change in the shape of the layer occur simultaneously and begin only as soon as the injection of the toroidal B-field is terminated at $t \approx 175\mu s$.

Comparison of the numerical results presented in Figures 2-5 to the published MRX experimental data suggests that the TRIM implementation of resistive, compressible MHD equations with radiative energy loss does a good job of reproducing the global characteristics of the MRX experiment. An X-point configuration is observed to evolve into a Y-shaped current layer, correlated with the initial increase of the peak J_ϕ in the layer. Once the long thin "steady-state" current sheet is established, the peak magnitude of J_ϕ slowly decays, while strong plasma heating in the layer is observed.

However, it should be noted that there are some experimental features that are not reproduced in the simulation. MRX experimental data suggests significant ac-

cumulation of plasma density in the "steady-state" reconnection layer (see Fig.8 of ref.[20]). This is not observed in the resistive MHD simulation. Furthermore, the collapse of the X-point reconnection to the Y-shaped current sheet (see Figure 3) observed both in the experiment and simulation, seems to take longer in the resistive MHD model.

4 Hall current, MHD symmetry and reconnection

It is inherent in the single-fluid MHD approximation, that the addition of the Hall current term to the resistive Ohm's law is responsible for accounting for the ion-electron mass difference in the limit $m_e/m_i \ll 1$ [28]. In fact, in the collisional steady state limit, it is easy to show that the simple resistive Ohm's law allows for the masses of the positive and negative charges in plasma to be equal. However, when the Hall current is included in the limit of $m_e/m_i \to 0$, velocities of the ion and electron fluids can be separated and ion inertia is accounted for.

It is easily observed, that the set of single-fluid MHD equations with simple resistive Ohm's law is symmetric under the reversal of all electro-magnetic variables. That is, if $\mathbf{B} \to -\mathbf{B}$, $\mathbf{J} \to -\mathbf{J}$ and $\mathbf{E} \to -\mathbf{E}$, then pressure p, density ρ and velocity field $\mathbf{v}$ remain unaffected. However, once the Hall current is included (see Eqs.1 - 5 with non-zero λ), this symmetry is destroyed. Now, lets qualitatively inspect what happens to the out-of-plain plasma flow and magnetic field components in 2D magnetic reconnection geometry under such a symmetry transformation.

As discussed earlier, the Hall term in the generalized Ohm's law has been shown to be responsible for localization of the reconnection layer to an X-point structure. The major signature of Hall mediated reconnection is the induced quadrupolar configuration of the out-of-plain B_ϕ^{Hall}-fields associated with poloidal currents that result from the separation of ion and electron scales. The superposition of pre-existing out-of-plain magnetic fields and this self-generated quadrupolar field is the effect we should investigate here.

To demonstrate, we apply our qualitative analysis to the MRX geometry. As shown in Figure 6, there are two cases to be considered:

(1) counter-helicity reconnection, where initially present out-of-plain B_ϕ-field is of opposite sense on the two sides of the reconnection site;

(2) co-helicity reconnection, where the out-of-plain guide B_ϕ-field is approximately uniform.

For the first case, lets consider the particular orientation of poloidal and toroidal

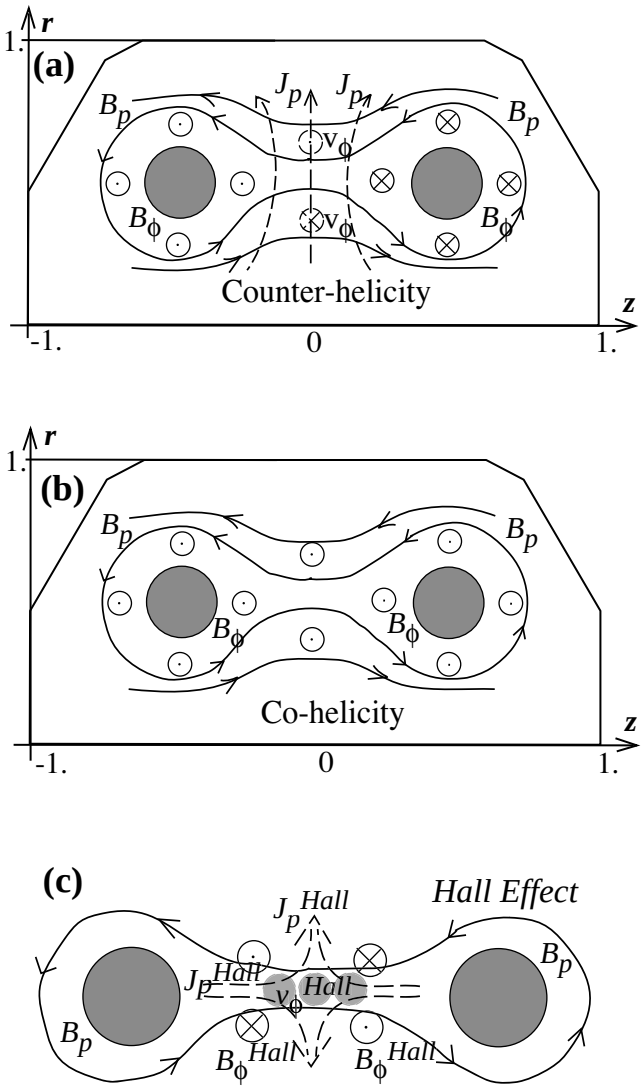

Figure 6: The schematic of toroidal flows resulting from various $\mathbf{J} \times \mathbf{B}$ forces in the MRX geometry: (a) counter-helicity MHD analysis; (b) co-helicity MHD analysis; (c) additional magnetic fields, plasma currents and flows resulting from the Hall effect and independent of the embedded toroidal B-fields.

magnetic fields, $\mathbf{B_p}, B_\phi$ shown in Fig.6(a). A poloidal current, $\mathbf{J_p}$ is present, associated with the embedded toroidal B_ϕ-fields. As a result, the $\mathbf{J} \times \mathbf{B}$ force, acting in the opposite direction above and below the reconnection region, generates opposing toroidal flows. (Note, the description above is equivalent to that of the slingshot effect given by Yamada, *et.al.*[29] and does not involve the Hall term.).

In the second case (see Fig.6(b)), the embedded toroidal B_ϕ-fields are such that no radial current should be induced along the $z = 0$ symmetry axis by the resistive effects alone. It follows, that in resistive MHD no significant toroidal flow should be expected on the $z = 0$ axis.

In Figure 6(c), we consider the additional toroidal B_ϕ^{Hall}-fields and associated poloidal $\mathbf{J}^{Hall}$ currents that are generated by the Hall term itself [7, 5]. These are independent of the orientation of the imposed B_ϕ and $\mathbf{B_p}$ and result in an additional toroidal $(\mathbf{J} \times \mathbf{B})_\phi^{Hall}$ force. The toroidal flow v_ϕ^{Hall} due to the interaction of the Hall current with the reconnecting field should be co-directed in all of the reconnection region and independent of B_ϕ embedded in the plasma.

The above analysis makes plausible the possibility of measuring and identifying the effects of the Hall term in experimental devices such as MRX. By simultaneously reversing the directions of initially imposed B_ϕ and $\mathbf{B_p}$, two effects should be observed:
(1) for counter-helicity reconnection, when the total embedded $\mathbf{B}$-field is reversed, the Hall driven toroidal flows should modify the otherwise unchanged radial profile of the plasma flow along the symmetry axis, $v_\phi(r, z = 0)$;
(2) the superposition of embedded B_ϕ and Hall induced B_ϕ^{Hall} should result in a radial shift of the contours of the total measured $B_\phi^{Total}(r, z)$ up or down depending on the orientation of the embedded B_ϕ.

The existing measurements of toroidal plasma flow in MRX in co- and counter-helicity configurations (see Fig.9 and Fig.10 of ref.[17]) are consistent with the qualitative analysis above.

5 Hall MHD Simulation results

As discussed above, we are unable to include the full magnitude of the Hall effect in our simulations of the MRX experiment. The results presented below are produced with $\lambda' = 3.2 \times 10^{-3}$, which is about 15% of the desired value. We address the scaling of the physical effects of the Hall term with the λ parameter later in this section.

We observe the counter-helicity Hall MHD simulation to have qualitatively the

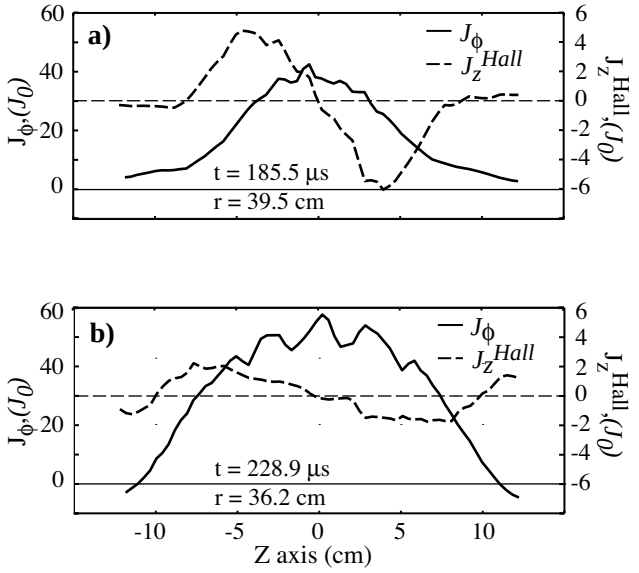

Figure 7: Profiles of reconnection J_ϕ and Hall current J_z^{Hall} versus z at (a) $t = 185.5\mu s$ and (b) $t = 228.9\mu s$ during the counter-helicity Hall MHD simulation ($J_0 = 16.0kA/m^2$). Note that different radial positions at different times are due to the slow radial motion of the reconnection layer.

same global dynamics and time-evolution as the resistive MHD results presented above. However, we also observe appearance of the Hall currents now embedded in the resistive MHD field structure. In the figures below, we were able to specifically extract the contribution of the Hall term to the total $\mathbf{B}$ and $\mathbf{J}$, as shown in Figure 6.

In Figure 7, we show the z-profiles of the reconnection current J_ϕ and Hall current J_z^{Hall} inside the layer at two different times: early during X-point reconnection at $t = 185.5\mu s$, and late in the Y-shaped layer at $t = 228.9\mu s$. In Figure 8, we also show radial profiles through the center of the reconnection layer of contributions of $\eta\mathbf{J}_\phi$ and $\lambda(\mathbf{J} \times \mathbf{B})_\phi^{Hall}$ to the out-of-plain reconnection electric field E_ϕ at those same times.

Taking a ratio of peak magnitudes of the plasma currents shown in Fig.7(a), we observe that during X-point reconnection the Hall current constitutes more than 10% of J_ϕ. Late in time, however, this ratio goes down to about 3% in Fig.7(b). A similar trend is observed in Figure 8, where the contribution of the Hall term to the total reconnection E-field relative to ηJ_ϕ goes from almost 10%

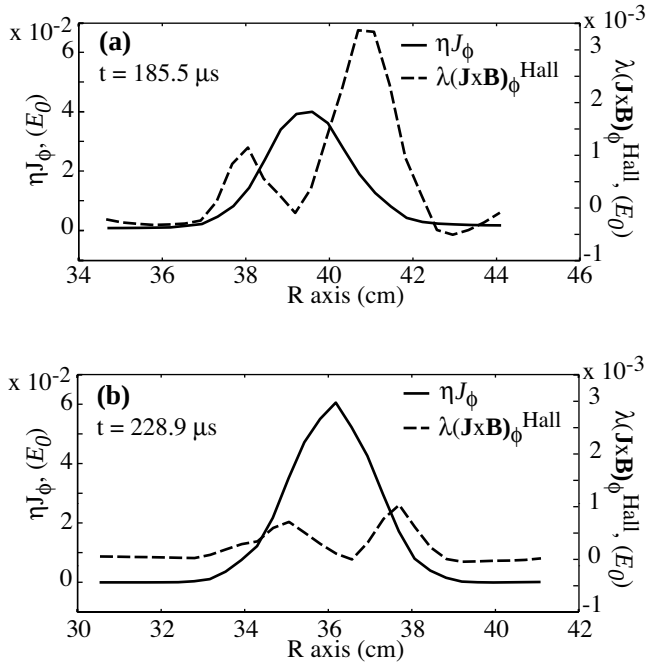

Figure 8: Radial profiles of the ηJ_ϕ and $\lambda(\mathbf{J} \times \mathbf{B})_\phi^{Hall}$ contributions to the total reconnection electric field E_ϕ through the center of the reconnection layer at (a) $t = 185.5\mu s$ and (b) $t = 228.9\mu s$ during the counter-helicity Hall MHD simulation ($E_0 = 1.035kV/m$).

to less than 2%. It should be noted, that in the MRX geometry the *global* evolution of B-fields influence the shape of the reconnection layer. That is, the boundary conditions at the flux-cores drive reconnection in such a way that late in time there is a strong tendency to end up with a Y-shaped reconnection layer, rather than an X-point, independent of the physical mechanism facilitating reconnection. Hall reconnection, on the other hand, tends to transform the layer into an open X-point configuration [7]. We, therefore, observe that the Hall effect is mediated during the steady-state MRX reconnection phase by the forced global evolution of the magnetic fields.

We now address the symmetry properties of Hall MHD, considered in the previous section. In Figure 9, we present the radial profiles of toroidal plasma flow calculated in two separate simulation runs, where we reverse all imposed electro-magnetic initial and boundary conditions for one run with respect to the other. In particular, in one run $\mathbf{B_p}$ is oriented counter-clockwise (as in Fig.6(a)),

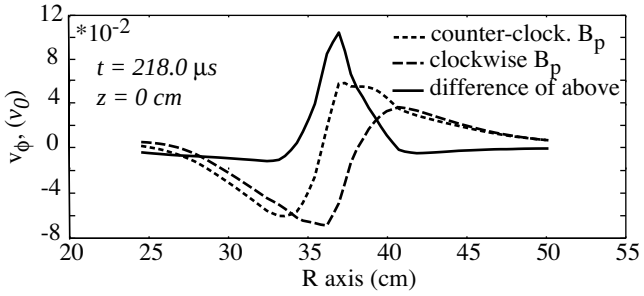

Figure 9: The two dashed lines show the radial profiles of toroidal flow v_ϕ for two separate counter-helicity Hall MHD simulation runs, where all imposed electromagnetic initial and boundary conditions are reversed with respect to each other ($v_0 = 69.0km/s$). The solid line is the difference of the two.

while in the other $\mathbf{B_p}$ is clockwise. On the same plot we show the difference between the two, which is twice the flow due to the Hall effect with all of the slingshot flow having canceled out. In each run the radial location of the current layer is identical and perfectly corresponds to the peak in the resulting v_ϕ^{Hall} profile (not shown).

We also attempted to conduct studies of the Hall MHD reconnection in the co-helicity configuration. However, as in the experiment [17, 21], we do not observe formation of a Y-shaped thin current layer during co-helicity reconnection. As shown in Figure 10, the thick X-shaped reconnection region eventually becomes O-shaped and turns into a spheromak. The Hall term is not seen to play any role in this transition.

Finally, to the issue of scaling of the Hall effect with the λ parameter. We have completed simulation runs with three different λ' values $\lambda' = 1.6 \times 10^{-3}; 2.4 \times 10^{-3}; 3.2 \times 10^{-3}$. In Figure 11, radial profiles of B_ϕ^{Hall} and v_ϕ^{Hall} across the counter-helicity reconnection layer for all three λ' values are shown late during the Y-layer phase of the simulation. The magnitude of the Hall effect at $t = 256\mu s$ is approximately proportional to the λ' parameter for those small values of λ'.

6 Conclusions

The two-dimensional resistive MHD model reproduces many features of the experimentally observed evolution of the magnetic fields and currents in MRX. Transition to the Y-shaped current layer from the initial X-point configuration

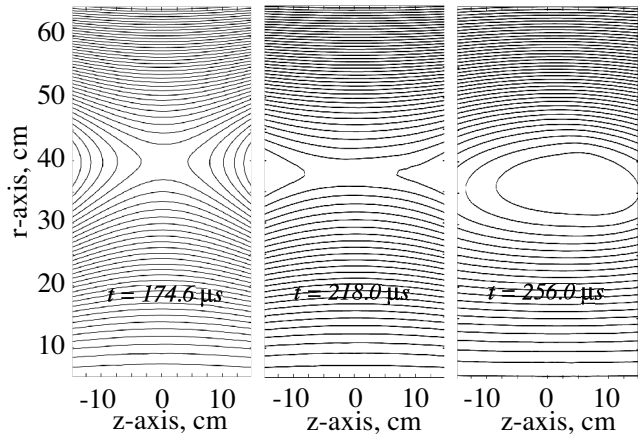

Figure 10: The evolution of poloidal magnetic flux from X-point to O-point reconnection region during co-helicity reconnection.

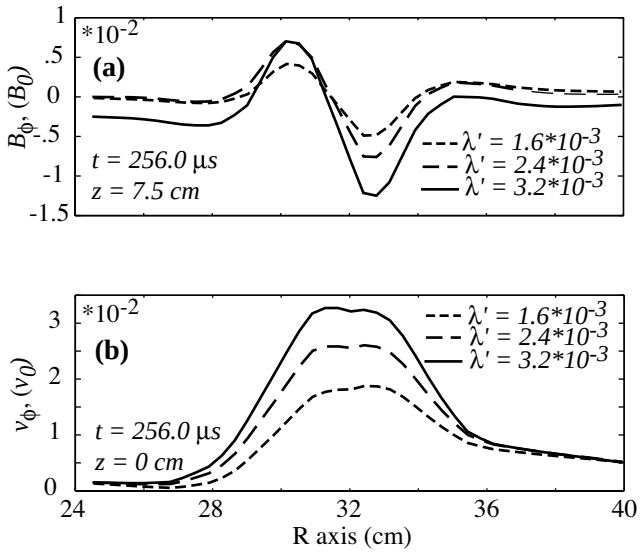

Figure 11: The radial profiles of (a) B_ϕ^{Hall} at $z = 7.5cm$ ($B_0 = 150Gauss$) and (b) v_ϕ^{Hall} at $z = 0cm$ ($v_0 = 69.0km/s$) for three values of the λ' parameter each very late during counter-helicity reconnection at $t = 256.0\mu s$.

is correlated with the increase in the reconnection current and with the termination of toroidal B-field generation at the flux-cores. Significant plasma heating is observed once the "steady-state" reconnection layer is established.

A careful comparison of the Hall MHD results to the baseline resistive MHD simulation uncovers the role of the Hall term in MRX counter-helicity reconnection. As shown in Fig.7 and Fig.8, even with λ' of only 15% of the desired value, the Hall effect is already responsible for about 10% of the out-of-plain electric field in the center of the reconnection region during the X-phase of the process. Although the exact scaling of the Hall effect with λ' cannot be extrapolated from Fig.11 during this early phase, it is apparent that the Hall effect should play a major role in the X-phase of MRX reconnection.

The transition to the long Y-shaped reconnection layer, forced by the global structure of the magnetic fields in MRX, is accompanied by the diminishing contribution of the Hall term to the reconnection E_ϕ-field. Using the scaling of Fig.11, we can estimate that late in time the Hall currents should only be about 10-15% of the reconnection current and thus do not significantly influence the magnetic structure or the effective resistivity.

As qualitatively described in Section 4 and numerically confirmed in Fig.9, we propose to conduct a "symmetry experiment" in MRX, by independently reversing the induced electro-magnetic fields and measuring the radial profiles of the plasma flow for all four combinations of the poloidal and toroidal **B**-field configurations of the counter-helicity reconnection. By combining the profiles, a direct measurement of the Hall effect in MRX should result.

In co-helicity reconnection, where the B_ϕ-field is observed to accumulate in the reconnection region, the layer develops an O-point and evolves into a spheromak. This is consistent with the experimentally observed evolution in this configuration[18, 20].

Acknowledgments

The authors would like to thank M. Yamada, H. Ji and A. Kuritsyn for assistance in understanding the experimental conditions in the MRX experiment, D.D. Schnack for making the TRIM code and some preliminary results available, and J. Breslau for useful discussions.

The computer calculations were performed at the National Energy Research Scientific Computing Center. This work was supported by the U.S. Department of Energy (DOE) Contract No. DE-AC020-76-CH03073 and under appointment

to the Fusion Energy Sciences Fellowship Program administered by Oak Ridge Institute for Science and Education under a contract between U.S.DOE and the Oak Ridge Associated Universities.

References

[1] A. Zeiler, D. Biskamp, J.F. Drake, B.N. Rogers, M.A. Shay, M. Scholer, J. Geophys. Res. **107**, 1230 (2002).

[2] W. Pei, R. Horiuchi, T. Sato, Phys. Rev. Lett. **87**, 235003 (2001).

[3] S.V. Bulanov, E. Yu. Echkina, I.N. Inovenkov, F. Pegoraro, V.V. Pichushkin, Plasma Phys. Reports **27**, 334 (2001).

[4] L. Yin, D. Winske, S.P. Gary, J. Birn, Phys Plasmas **9**, 2575 (2002).

[5] J. A. Breslau and S.C. Jardin, Comp. Physics Comm., [to be published 2003]; PPPL-3600 (2001).

[6] J. Birn, J.F. Drake, M.A. Shay, B.N. Rogers, R.E. Denton, M. Hesse, M. Kuznetsova, Z.W. Ma, A. Bhattacharjee, A. Otto, P.L. Pritchett, J. Geophys. Res. **106**, 3715 (2001).

[7] B.N. Rogers, R.E. Denton, J.F. Drake, M.A. Shay, Phys. Rev. Lett. **87**, 195004 (2001).

[8] M.A. Shay, J.F. Drake, B.N. Rogers, R.E. Denton, Geophys. Res. Lett. **26**, 2163 (1999).

[9] X. Wang, A Bhattacharjee, Z.W. Ma, Phys. Rev. Lett. **87**, 265003 (2001).

[10] D. Biscamp, E. Schwarz, Phys. Plasmas **8**, 4729 (2001).

[11] S.I. Syrovatsky, Sov. Phys. JETP **33**, 933 (1971).

[12] M. Oieroset, T.D. Phan, M. Fujimoto, R.P. Lin, R.P. Lepping, Nature (London) **412**, 414 (2001).

[13] F.S. Mozer, S.D. Bale, T.D. Phan, Phys. Rev. Lett. **89**, 015002 (2002).

[14] M.R. Brown, Phys. Plasmas **6**, 1717 (1999).

[15] M.R. Brown, C.D. Cothran, M. Landerman, D. Schlossberg, W.H. Matthaeus, G. Qin, V.S. Lukin, T. Gray, Phys. Plasmas **9**, 2077 (2002)

[16] Y. Ono, M. Inomoto, T. Okazaki, Y. Ueda, Phys. Plasmas **4**, 1953 (1997).

[17] S.C. Hsu, T.A. Carter, G. Fiksel, H. Ji, R.M. Kulsrud, M. Yamada, Phys. Plasmas **8**, 1916 (2001).

[18] M. Yamada, H. Ji, S. Hsu, T. Carter, R. Kulsrud, F. Trintchouk, Phys. Plasmas **7**, 1781 (2000)

[19] T. Carter, *Dissertation*, Princeton University (2001).

[20] H. Ji, M. Yamada, S. Hsu, R. Kulsrud, T. Carter, S. Zaharia, Phys. Plasmas **6**, 1743 (1999).

[21] M. Yamada, H. Ji, S. Hsu, T. Carter, R. Kulsrud, N. Bretz, F. Jobes, Y. Ono, F. Perkins, Phys. Plasmas **4**, 1936 (1997).

[22] J. Egedal, A. Fasoli, D. Tarkowski, A. Scarabosio, Phys. Plasmas **8**, 1935 (2001)

[23] V.S. Lukin, G. Qin, W.H. Matthaeus, M.R. Brown, Phys. Plasmas **8**, 1600 (2001).

[24] G. Qin, V.S. Lukin, C.D. Cothran, M.R. Brown, W.H. Matthaeus, Phys. Plasmas **8**, 4816 (2001).

[25] D.D. Schnack, I. Lotatti, Z. Mikic, P. Satyanarayana, J. Comp. Phys. **140**, 71 (1998).

[26] D.E. Post, R.V. Jensen, C.B. Tarter, W.H. Grasberger, W.A. Lokke, Atom. Data and Nucl. Data Tables, **20**, 397 (1977)

[27] T.-H. Watanabe, T. Hayashi, T. Sato, M. Yamada, H. Ji, Phys. Plasmas **6**, 1253 (1999).

[28] See, e.g., F. F. Chen, *Plasma Physics and Controlled Fusion, 2nd ed.* (Plenum Press, New York, 1984)

[29] M. Yamada, Y. Ono, A. Hayakawa, M. Katsurai, F. W. Perkins, Phys. Rev. Lett. **65**, 721 (1990).

External Distribution

Plasma Research Laboratory, Australian National University, Australia
Professor I.R. Jones, Flinders University, Australia
Professor João Canalle, Instituto de Fisica DEQ/IF - UERJ, Brazil
Mr. Gerson O. Ludwig, Instituto Nacional de Pesquisas, Brazil
Dr. P.H. Sakanaka, Instituto Fisica, Brazil
The Librarian, Culham Laboratory, England
Mrs. S.A. Hutchinson, JET Library, England
Professor M.N. Bussac, Ecole Polytechnique, France
Librarian, Max-Planck-Institut für Plasmaphysik, Germany
Jolan Moldvai, Reports Library, MTA KFKI-ATKI, Hungary
Dr. P. Kaw, Institute for Plasma Research, India
Ms. P.J. Pathak, Librarian, Insitute for Plasma Research, India
Ms. Clelia De Palo, Associazione EURATOM-ENEA, Italy
Dr. G. Grosso, Instituto di Fisica del Plasma, Italy
Librarian, Naka Fusion Research Establishment, JAERI, Japan
Library, Plasma Physics Laboratory, Kyoto University, Japan
Research Information Center, National Institute for Fusion Science, Japan
Dr. O. Mitarai, Kyushu Tokai University, Japan
Library, Academia Sinica, Institute of Plasma Physics, People's Republic of China
Shih-Tung Tsai, Institute of Physics, Chinese Academy of Sciences, People's Republic of China
Dr. S. Mirnov, TRINITI, Troitsk, Russian Federation, Russia
Dr. V.S. Strelkov, Kurchatov Institute, Russian Federation, Russia
Professor Peter Lukac, Katedra Fyziky Plazmy MFF UK, Mlynska dolina F-2, Komenskeho Univerzita, SK-842 15 Bratislava, Slovakia
Dr. G.S. Lee, Korea Basic Science Institute, South Korea
Institute for Plasma Research, University of Maryland, USA
Librarian, Fusion Energy Division, Oak Ridge National Laboratory, USA
Librarian, Institute of Fusion Studies, University of Texas, USA
Librarian, Magnetic Fusion Program, Lawrence Livermore National Laboratory, USA
Library, General Atomics, USA
Plasma Physics Group, Fusion Energy Research Program, University of California at San Diego, USA
Plasma Physics Library, Columbia University, USA
Alkesh Punjabi, Center for Fusion Research and Training, Hampton University, USA
Dr. W.M. Stacey, Fusion Research Center, Georgia Institute of Technology, USA
Dr. John Willis, U.S. Department of Energy, Office of Fusion Energy Sciences, USA
Mr. Paul H. Wright, Indianapolis, Indiana, USA

The Princeton Plasma Physics Laboratory is operated
by Princeton University under contract
with the U.S. Department of Energy.

Information Services
Princeton Plasma Physics Laboratory
P.O. Box 451
Princeton, NJ 08543

Phone: 609-243-2750
Fax: 609-243-2751
e-mail: pppl_info@pppl.gov
Internet Address: http://www.pppl.gov